Science and Technology Indonesia
e-ISSN:2580-4391 *p*-ISSN:2580-4405
Vol. 11, No. 2, April 2026

Research Paper

Enhancing Chitosan-Carboxymethyl Chitosan Composite Film Properties By Silver Nanoparticles Grafting For *Acne vulgaris*

Septian Dwi Mulyana[1], Muh. Agus Syamsur Rijal[2,3], Retno Sari[2,3*]

[1]*Pharmacy Study Program, Faculty of Health Sciences, Universitas Muhammadiyah Lamongan, East Java, 62264, Indonesia*
[2]*Department of Pharmaceutical Sciences, Faculty of Pharmacy, Universitas Airlangga, Surabaya, East Java, 60115, Indonesia*
[3]*Pharmaceutics and Delivery Systems for Drugs, Cosmetic, and Nanomedicine Research Group, Faculty of Pharmacy, Universitas Airlangga, Surabaya, East Java, 60115, Indonesia*
*__Corresponding author__: retno-s@ff.unair.ac.id

Abstract
Silver nanoparticles (AgNPs) have been widely used in developing antibacterial preparations. AgNPs are used in film preparation to enhance the film's antibacterial properties. The combination of natural polymers is an effective strategy to enhance mechanical properties, prolong degradation time, preserve gas and vapor permeability, and maintain biocompatibility. This research aims to develop an AgNP-chitosan-carboxymethyl chitosan (CMChi) nanocomposite film that exhibits desirable physical properties and enhances antibacterial activity by incorporating AgNPs. Chitosan-CMChi composite films were prepared using the solvent casting method. Characterization and antibacterial tests using *Propionibacterium acnes* (*P. acnes*) were carried out for $AgNO_3$ and AgNP-chitosan-CMChi nanocomposite films. The results showed that a 1 mM $AgNO_3$ solution with 1% lime powder at pH 9 was the optimal formulation for AgNP formation, exhibiting an absorbance of 4.631 at 408.1 nm, a particle size of 68.4 nm, and antibacterial activity. To optimize the chitosan-CMChi composite film, a formula of 1.5% chitosan and 1.5% CMChi was selected, yielding a tensile strength value of 0.514 MPa. The AgNP solution was then added. In the AgNP-chitosan-CMChi nanocomposite film, it was observed that increasing the AgNP volume affected the mechanical strength of the film. The antibacterial activity of the AgNP-chitosan-CMChi nanocomposite film increased with the AgNP concentration. Combining AgNPs with the chitosan-CMChi polymer yields nanocomposite films with good physical properties and enhanced antibacterial activity against *P. acnes* compared with films without AgNPs.

Keywords
Silver Nanoparticles, Nanocomposite Film, Chitosan, Carboxymethyl Chitosan, Antibacterial

Received: 13 December 2025, Accepted: 20 February 2026
https://doi.org/10.26554/sti.2026.11.2.559-568

1. INTRODUCTION

Many antibacterial materials are made from metal nanoparticles such as silver (Ag) and gold (Au). Silver nanoparticles (AgNPs) are known to exhibit strong antibacterial activity, even at lower concentrations than other metals (Chadha et al., 2014). Because they possess a large surface area relative to their volume and small size, AgNPs easily penetrate bacterial cell walls (Alafandi et al., 2021; Alshamari et al., 2026; Kinoan, 2025). Based on the antibacterial mechanism of AgNP, free silver ions (Ag^+) released from AgNPs can efficiently inhibit bacterial growth (Mohamed and Madian, 2020). Synthesizing AgNPs using green methods, such as plants as reducing agents, offers significant advantages over other AgNP synthesis methods, as reported in recent plant-mediated nanoparticle fabrication studies (Fithri et al., 2025; Madaniyah et al., 2025). Functional groups in plant biomolecules, such as flavonoids, terpenoids, polyphenols, alkaloids, saponins, and tannins, can act as reducing agents, forming Ag+ ions that reduce to Ag^0 (Ceballos et al., 2021). These biomolecules are found in various plant parts, including leaves, roots, seeds, stems, and flowers (Zimet et al., 2019). Different synthesis conditions result in nanoparticles with varying characteristics, including stability and antibacterial performance (Madaniyah et al., 2025). Therefore, it is essential to identify the desired physicochemical characteristics of nanoparticles to determine the parameters used in synthesis. Some parameters include reaction time, temperature, pH, $AgNO_3$ concentration, and reducing agent concentration (Nugraheni et al., 2018).

Films have been developed as a new approach for topical drug delivery due to their thin form and flexible nature, and are easier to use (Karki et al., 2016; Takeuchi et al., 2018). Adding AgNPs (nanocomposites) to the film matrix can significantly affect the film's mechanical properties and transparency

(Nishigaki et al., 2012). Chitosan can form films with favorable mechanical strength due to strong ionic interactions between its negatively charged hydroxyl groups and positively charged amine groups. It can form transparent films that enhance moisture-barrier performance (Dayarian et al., 2014; Psimadas et al., 2012). Chitosan is widely applied in different areas, such as cosmetic products and pharmaceutical drug delivery systems, by enhancing formulation stability, acting as a chelating agent, promoting healing, such as tissue growth, and inhibiting fibrosis (Cazón et al., 2017). The flexibility of chitosan films can be increased by adding other polymers and plasticizers. Since chitosan has amine ($-NH_2$) and hydroxyl ($-OH$) groups in its structure, it is well-suited for various cross-linking reactions, including with other polymers and AgNPs (Ag^+) (Abraham et al., 2016).

The physical and mechanical characteristics of chitosan films can be enhanced by blending chitosan with other polymers, such as poly(vinyl alcohol) (PVA), carboxymethyl cellulose (CMChi), hydroxypropyl methylcellulose (HPMC), polylactic acid (PLA), and carboxymethyl chitosan (CMChi) (Bahsaine et al., 2023; Elgharbawy et al., 2024; Wardhono et al., 2022). CMChi is a water-soluble biopolymer derived from chitosan by chemical modification, characterized by its high hydrophilicity. It is produced by incorporating carboxymethyl groups into chitosan, yielding an amphoteric polymer with both $-NH_2$ and $-COOH$ groups along the chain. In addition to its excellent solubility, CMChi is biocompatible and biodegradable, exhibits film-forming ability, and possesses antibacterial properties (Ounkaew et al., 2020; Savencu et al., 2021; Yang et al., 2020). The combination of natural polymers aims to improve mechanical properties, extend degradation time, maintain gas and water vapor permeability, and maintain product biocompatibility (Li et al., 2024). The physical and mechanical characteristics of composite films can be enhanced by blending chitosan with CMChi (Rozilah et al., 2020).

By considering these aspects, this research aims to develop an AgNP-grafted chitosan-CMChi nanocomposite film formulation that exhibits good physical properties and enhances antibacterial activity, particularly against acne-causing bacteria. The research involves synthesizing AgNP-chitosan-CMChi nanocomposite films with varying AgNP concentrations to improve their properties and antibacterial activity. These films should exhibit mechanical properties that are not easily brittle when applied and a pH that does not irritate the skin. The nanocomposite films were evaluated for their physical and mechanical characteristics and for antibacterial activity against *Propionibacterium acnes (P. acnes)*.

2. EXPERIMENTAL SECTION

2.1 Materials

2.1.1 Chemicals and Reagents

$AgNO_3$ (Sigma-Aldrich, USA), lime, chitosan (100 cps) (Biotech Surindo), carboxymethyl chitosan (CMChi) (Sigma-Aldrich, USA), glacial acetic acid (Merck, Germany), distilled water, propylene glycol (PT. Brataco, Indonesia), nutrient broth (Merck, Germany), nutrient agar (Merck, Germany), NaOH (sodium hydroxide) (Merck, Germany), and *Propionibacterium acnes* bacteria (ATCC 11827) from Center of Health Laboratory, Surabaya, Indonesia (Balai Besar Laboratorium Kesehatan).

2.2 Methods

2.2.1 Synthesis of AgNP at pH 9

A 1% lime juice powder solution and a 1 mM $AgNO_3$ solution were prepared separately. Then, 25 mL of the lime juice solution was mixed with 25 mL of the $AgNO_3$ solution, and the mixture was stirred at 250 rpm for 1 hour. The pH of the mixture was adjusted to 9 using 1 N NaOH, followed by continuous stirring at 250 rpm at room temperature for another hour. Finally, the resulting AgNP solution was heated in an oven at 60°C for 2 hours (Mulyana et al., 2024).

2.2.2 Preparation of Chitosan-CMChi Composite Film

Chitosan was first dissolved in 1% acetic acid, while CMChi was prepared in distilled water. The two solutions were then mixed under constant stirring. Propylene glycol was added gradually until a uniform mixture was obtained, and the final volume was adjusted to 100 mL with distilled water. An aliquot of 5 mL was poured into a 5 cm diameter petri dish and dried at 40°C for 5 hours. After drying, the films were removed and kept in airtight containers for subsequent characterization (Dayarian et al., 2014; Zhang et al., 2015).

2.2.3 Preparation of AgNP-Chitosan-CMChi Nanocomposite Film

Chitosan was prepared in 1% acetic acid, while CMChi was dissolved in distilled water, and both solutions were stirred continuously at 250 rpm for 30 minutes. Propylene glycol and the AgNP solution were then added to the mixture, and the final volume was adjusted to 100 mL with distilled water. A 5 mL portion of the solution was poured into a 5 cm diameter petri dish and dried at 40°C for 5 hours. The resulting nanocomposite films were collected and stored in airtight containers for further analysis (Tang et al., 2022).

2.2.4 Characterization of Chitosan-CMChi Composite and AgNP-Chitosan-CMChi Nanocomposite Film

The dried film formulation underwent physical and mechanical evaluations. FTIR analysis was performed to determine functional groups and verify possible chemical interactions. Surface morphology was examined using SEM. In addition, film thickness (mm), folding endurance, moisture content (%), swelling index (%), tensile strength (MPa), elongation at break (%), and Young's modulus (N/mm^2) were measured to assess the film's elasticity and mechanical performance (Zhang et al., 2015).

2.2.5 Antibacterial Activity Test

The antibacterial activity of the film was assessed using the agar diffusion method against *Propionibacterium acnes*. Warm nutrient media were prepared and poured into sterile petri

dishes, containing 12 mL (base layer) and 8 mL (seed screen), to which 10 μl of P. acnes bacterial inoculum had been added. The AgNP-Chitosan-CMChi nanocomposite film was cut into a 5 mm diameter and then placed on the media. The media were incubated at 37°C for 24 hours, and the inhibition zone formed was measured. Clindamycin was used as a positive control (Awaluddin et al., 2022).

2.2.6 Data Analysis

The properties of the nanocomposite films, including tensile strength and antibacterial activity, were statistically analyzed using a One-way ANOVA at the 95% confidence level, followed by a Tukey HSD post hoc test. All tests were carried out in triplicate unless specified otherwise, and the data are presented as mean ± standard deviation (SD). Statistical analysis was applied to determine significant differences between samples, with significance defined at p <0.05 (Gurvich and Naumova, 2021; Montgomery, 2019; Zar, 2010).

3. RESULTS AND DISCUSSION

3.1 Characteristics of Silver Nanoparticles: Spectrophotometer & Delsa Nano

The absorbance values and particle size of AgNPs synthesized using lime juice powder extract (1%) with 1.0 M $AgNO_3$ solution at pH 9. The UV–Vis analysis showed a distinct absorption peak at 408.1 ± 0.02 nm, corresponding to the typical surface plasmon resonance (SPR) band of silver nanoparticles. This result confirms the successful formation of AgNPs, as absorption in the 400–450 nm range is commonly associated with nanoscale silver. The corresponding absorbance value (4.631 ± 0.11) indicates a relatively high intensity, suggesting efficient nanoparticle formation and stability. Dynamic Light Scattering (DLS) analysis revealed that the synthesized AgNPs had an average hydrodynamic diameter (D_{ave}) of 63.4 ± 1.40 nm, with a polydispersity index (PDI) of 0.251 ± 0.04, indicating a relatively narrow particle size distribution and acceptable nanoparticle homogeneity. In addition, a PDI value approaching 0 indicates a homogeneous particle size, whereas a PDI value <0.3 indicates a heterogeneous particle size (Danaei et al., 2018; Hoseini et al., 2023). The particle size obtained falls within the nanometer scale, supporting the UV–Vis results. Moreover, the PDI value, which is close to 0.2, suggests a narrow size distribution and acceptable homogeneity of the nanoparticle population. The wavelength and absorption intensity of the SPR phenomenon depend on several factors that can affect the electron charge density at the particle's surface. Some of these factors include the type of metal, particle size, shape, structure, and the medium's dielectric constant. Increasing the concentration of lime as a reducing agent can accelerate the formation of AgNPs because a greater availability of biomolecules, such as flavonoids, saponins, and tannins, acts as a reducing agent, capping agent, and stabilizer, thereby protecting the nanoparticles from aggregation (Alafandi et al., 2021; Chadha et al., 2014). Based on the formation mechanism, silver ions (Ag^+) will receive electrons from the reducing agent, become metal (Ag^0), and form AgNPs.

UV–Vis and DLS results verified the successful synthesis of AgNPs and provided information on their optical properties and hydrodynamic diameter in colloidal form; these data reflect the nanoparticle characteristics before incorporation into the film. After being embedded within the chitosan–CMChi matrix, the nanoparticles interact with the polymer chains, which can modify their apparent size, distribution, or detectability in the solid state (Angastiniotis et al., 2021; Harun-ur Rashid and Foyez, 2025). The SEM images in this study primarily reflect the morphological features of the composite films; however, individual AgNPs are not distinctly visible due to polymer coverage and limitations in SEM resolution for detecting small, embedded nanoparticles. Similar observations have been reported in other chitosan-based nanocomposite systems, in which AgNPs are often encapsulated within or distributed throughout the polymer network, making direct visualization challenging. Therefore, although the presence of AgNPs influences the surface texture and structural uniformity of the films, confirming their exact spatial distribution typically requires higher-resolution or element-specific methods such as TEM or EDS mapping (Abbasian et al., 2020; Kora and Rastogi, 2021; Li, 2023; Ramezani et al., 2022).

3.2 Characteristics of Chitosan-CMChi Composite Film

3.2.1 Organoleptics

Based on organoleptic evaluation, all chitosan-CMChi composite film formulations (F1, F2, and F3) exhibited similar physical characteristics. Each formulation appeared as a transparent, yellowish film. The surface texture of all films was smooth, indicating good polymer miscibility and homogeneity. Furthermore, the films were flexible and not easily torn, suggesting adequate interaction between chitosan and CMChi, resulting in strong film integrity. The essential considerations for choosing this formula are that it forms a film, has a smooth, even surface, peels off easily, and does not tear easily. The following tests were conducted to evaluate the characteristics of the chitosan-CMChi composite film, including organoleptic tests, pH change tests, thickness, foldability, moisture content, swelling index, tensile strength, elongation at break, and Young's modulus.

3.2.2 Spectroscopy ATR-FTIR Analysis

Based on Figure 1, the spectral profile of the chitosan-CMChi composite film is identical. At a wave number of 3425.58 cm^{-1}, absorption from the stretching vibration of the –OH group overlaps with the stretching absorption band of the –NH group, forming a broader band compared to chitosan alone. This indicates an increase in the –OH group, attributed to the addition of a carboxylic group (–COOH) (Hadi et al., 2023; He et al., 2015). The vibrations of the C−H group appear at wave numbers 2878.64 – 2972.48 cm^{-1}. The vibration of the C=O carbonyl group in amide and the N−H bond is indicated by absorptions at wave numbers 1649.84 cm^{-1} and

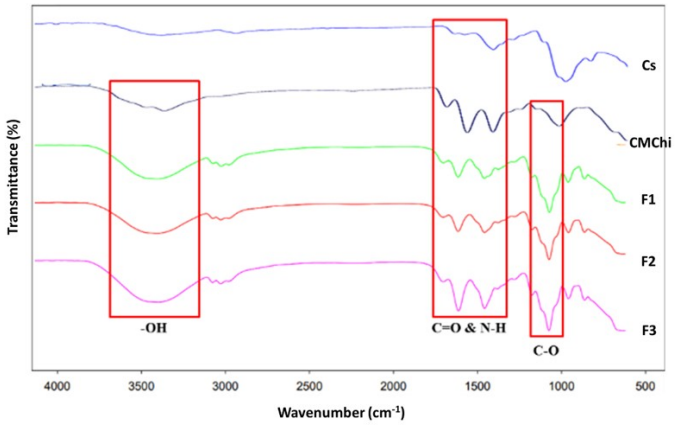

Figure 1. Infrared Spectra of Chitosan-CMChi Composite Film with CMChi Concentration of F1 (0.5%), F2 (1%), and F3 (1.5%)

1565.05 cm^{-1}, respectively (Ceballos et al., 2021; Mohamed and Madian, 2020).

Table 1. Composition of Chitosan and CMChi Composite Film

Material	Function	Concentration (%)		
		F1	F2	F3
Chitosan	Polymer	1.5	1.5	1.5
CMChi	Polymer	0.5	1	1.5
Acetic Acid 1%	Solvent	40	40	40
Propylene Glycol	Plasticizer	7	7	7
Aquadest	Solvent	100	100	100

3.2.3 SEM

Encapsulation based on the SEM results in Figure 2, the chitosan-CMChi composite film exhibits a flat, smooth, and non-porous surface, indicating a compact polymer chain arrangement that does not alter the film's microstructure (Zimet et al., 2019).

In this study, SEM was primarily used to examine the surface and cross-sectional morphology of the nanocomposite films, rather than to quantitatively measure the particle size or dispersion of AgNPs. Due to the polymeric nature of the chitosan–CMChi matrix, individual AgNPs may be embedded within the polymer network and covered by the polymer chains, thereby limiting their direct visualization by SEM. Although direct visualization of interfacial interactions between AgNPs and the polymer matrix was not possible using SEM, the observed changes in film surface morphology after AgNP incorporation indirectly suggest the presence of interactions between AgNPs and the chitosan–CMChi matrix. Similar observations have been reported in previous studies, where SEM images of polymer–AgNP nanocomposites provided qualitative morphological information, while nanoparticle localization and dispersion required complementary techniques such as transmission electron microscopy (TEM) or elemental mapping (EDS) (Mohamed and Madian, 2020; Yang et al., 2020).

Table 2. Composition of Nanocomposite AgNP-Chitosan-CMChi Film

Material	Fn0	Fn1	Fn2	Fn3
AgNP (mM)	0	0.25	0.375	0.50
Chitosan (%b/v)	1.5	1.5	1.5	1.5
CMChi (%b/v)	1.5	1.5	1.5	1.5
Acetic Acid 1% (%v/v)	40	40	40	40
Propylene Glycol (%v/v)	7	7	7	7
Aquadest ad (ml)	100	100	100	100

3.2.4 Physical and Chemical Properties of Chitosan-CMChi Composite Film

As presented in Table 3, the thickness of the chitosan–CMChi composite film increases with increasing CMChi concentration, ranging from 0.07 to 0.11 mm for concentrations of 0.5% to 1.5%. Film thickness is directly related to film weight; as thickness increases, so does film weight. From these results, the combination of the two polymers produces a greater increase in film thickness than either polymer alone. Additionally, chitosan retains water molecules, thereby contributing to a thicker film (Nugraheni et al., 2018). The acceptable range of film thickness is 0.05–1 mm (Karki et al., 2016). The foldability test aims to determine a film's durability when folded, flexibility during use, and elasticity (Takeuchi et al., 2018). The foldability test results for chitosan-CMChi composite films indicate that all films fold more than 300 times without damage or tearing. The polymer concentration influences the folding strength (Nishigaki et al., 2012). The combination of chitosan and CMChi enhances the film's strength, making it more tear-resistant. The interaction between the −OH and −NH groups enhances the film's strength (Dayarian et al., 2014). The requirement for good film folding strength is a folding resistance >300× (Psimadas et al., 2012). A high folding strength value indicates that the film has excellent mechanical properties. Therefore, all formulas demonstrate good foldability.

The moisture content of the chitosan-CMChi composite film was analyzed to determine the amount of water retained within the film matrix. The results of the moisture content test are presented in Table 3. The moisture content of the chitosan-CMChi composite film ranges from 9.31% to 12.92%. An increase in CMChi concentration results in a higher moisture content in the film. The hydrophilic properties of the −OH and −COOH groups in chitosan and CMChi contribute to the composite film's increased water content (Cazón et al., 2017; Zimet et al., 2019). This increase in moisture content reduces the film's tensile strength; the lower the moisture content, the greater the film's mechanical strength, as stronger hydrogen bonds form (Abraham et al., 2016). The swelling index reflects the film's ability to absorb wound exudate and

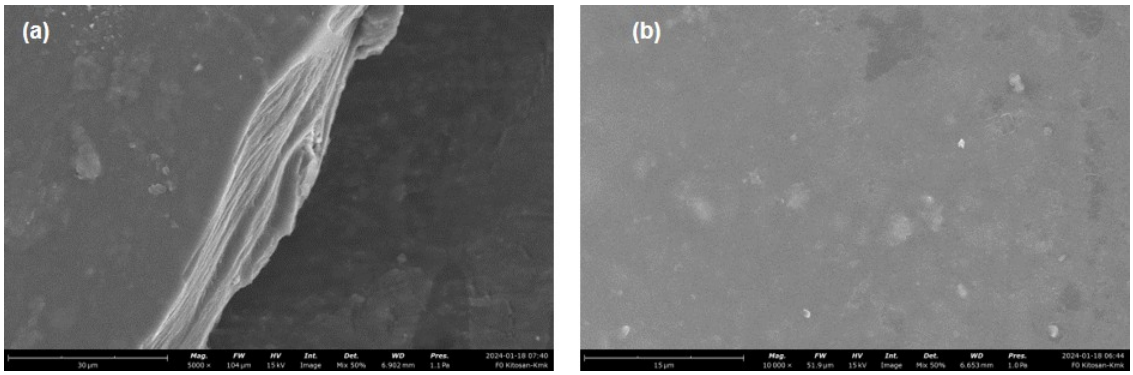

Figure 2. SEM Test Results of Chitosan-CMChi Composite Film: (a). Cross-Section and (b). Surface at 1000× Magnification

Table 3. The Mechanical Properties of Chitosan-CMChi Composite Film with a CMChi Concentration of F1 (0.5%), F2 (1%), and F3 (1.5%)

Evaluation	Formula		
	F1	F2	F3
Thickness (mm)	0.07 ± 0.01	0.10 ± 0.00	0.11 ± 0.01
Foldability	>300	>300	>300
Moisture Content (%)	9.31 ± 0.09	11.11 ± 0.16	12.92 ± 0.04
Swelling Index (%)	698.45 ± 0.32	753.59 ± 0.54	822.72 ± 0.61
Tensile Strength (MPa)	0.276 ± 0.00	0.389 ± 0.03	0.514 ± 0.06
Elongation at break (%)	57.28 ± 5.12	57.57 ± 5.35	58.31 ± 3.60
Young's Modulus (N/mm^2)	1.835 ± 0.61	1.916 ± 0.33	4.658 ± 0.82

expand, which is crucial for optimizing drug release. The chitosan–CMChi composite films showed swelling index of 698.45–822.72%, with statistical analysis (ANOVA, p <0.05) confirming significant differences among the formulas. Higher CMChi concentrations increased the swelling index by promoting interactions between carboxyl (−COOH) and amino ($-NH_2$) groups, thereby enhancing water absorption and film flexibility. The tensile strength of the composite films ranged from 0.276 to 0.514 MPa. ANOVA results (p = 0.002) indicated that higher CMChi concentrations, especially 1.5%, significantly increased tensile strength via hydrogen bonding and electrostatic interactions between polymer chains, resulting in stronger, more cohesive films. Elongation at break values ranged from 57.28% to 58.31%, indicating good flexibility, as all values exceeded 15%. Statistical analysis (p >0.05) revealed no significant difference among formulas, suggesting that all CMChi levels provided similar elasticity. The use of propylene glycol as a plasticizer further reduced brittleness and enhanced film flexibility. Young's modulus values ranged from 1.835-4.538 N/mm^2, with ANOVA (p = 0.006) indicating significant differences among formulas. The 1.5% CMChi concentration produced stronger and less brittle films. Overall, increasing CMChi concentration improved mechanical strength and elasticity due to synergistic interactions between chitosan and CMChi polymers.

3.3 Characteristics of AgNP-Chitosan-CMChi Nanocomposite Films

3.3.1 Organoleptics

The organoleptic evaluation of AgNP–chitosan–CMChi nanocomposite films with varying AgNP concentrations showed that the films appeared brownish clear, had a slightly sour odor, and possessed a smooth texture that was not easily torn. These results indicate that increasing the AgNP concentration within the studied range did not cause significant changes in the films' visual appearance, odor, or texture.

3.3.2 Spectroscopy ATR-FTIR Analysis

Figure 3 shows that the AgNP-chitosan-CMChi nanocomposite films have identical spectral profiles. At a wave number of 3425.58 cm^{-1}, there is an absorption of the stretching vibration of the −OH group, which overlaps with the stretching vibration absorption of −NH in Carboxymethyl chitosan, which is broader than that of chitosan. This indicates that there has been an increase in the -OH group originating from the addition of the carboxylate group (−COOH) (Hadi et al., 2023; He et al., 2015). Vibrations from the C−H group are seen at wave numbers 2878.64-2972.48 cm^{-1}. The carbonyl group C=O vibrations in amide and N−H are indicated by absorption at wave numbers 1649.84 cm^{-1} and 1565.05 cm^{-1}. The shift in the chitosan absorption band around 1585.71 cm^{-1} to 1565.05 cm^{-1}, which corresponds to the stretching of the N−H group,

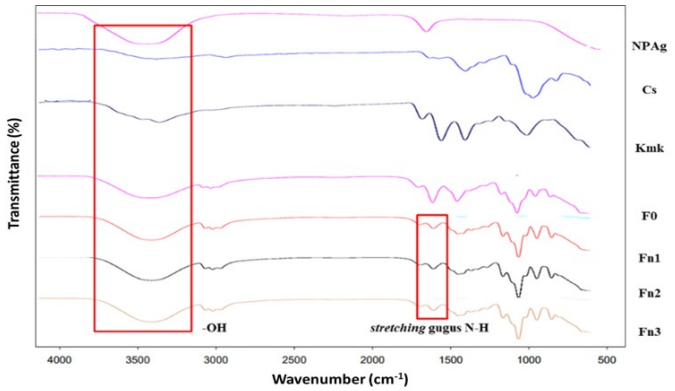

Figure 3. ATR Spectra of AgNP-Chitosan-CMChi Nanocomposite Films with Different AgNP Concentrations: Fn1 (0.25 mM), Fn2 (0.375 mM), and Fn3 (0.5 mM)

is caused by the interaction between AgNP and the N−H group in chitosan. The N−H bond of the amide in chitosan can act as a capping agent to maintain the stability of AgNP (Ceballos et al., 2021; Mohamed and Madian, 2020).

3.3.3 SEM

Based on the SEM results in Figure 4, the cross-section of the AgNP-chitosan-CMChi nanocomposite films exhibited an uneven morphology with several pores and micro-cracks, which may be attributed to polymer chain expansion and rearrangement induced by interactions with AgNPs (Susilowati et al., 2021). SEM analysis in this study was primarily intended to evaluate surface and cross-sectional morphology rather than to identify the embedded nanoparticles chemically.

3.3.4 Physical and Chemical Properties of AgNP-Chitosan-CMChi Nanocomposite Film

A swelling index test was conducted to determine the ability of the AgNP-chitosan-CMChi nanocomposite film to absorb wound fluid and exudates (Savencu et al., 2021). The swelling index of AgNP-chitosan-CMChi nanocomposite films ranges from 561.45% to 912.13%. To determine the effect of different AgNP concentrations on the swelling index of AgNP-chitosan-CMChi nanocomposite films. The statistical test results showed that p-values <0.05 indicate that all AgNP concentrations differ significantly. The results show that the three film formulas have a higher water absorption capacity than the chitosan-CMChi composite film. The swelling index results are also influenced by the degree of cross-linking. A high and appropriate level of cross-linking can increase hydrogel water retention, whereas a three-dimensional network with poor cross-linking will decrease film water retention. In the presence of acetic acid vapor, the $-COO^-$ groups in CMChi are protonated to $-COOH$, while the $-NH_2$ groups in chitosan become $-NH_3^+$. These changes promote electrostatic interactions that generate a densely crosslinked network, thereby enhancing water retention within the film (Ounkaew et al., 2020; Yang et al., 2020). Additionally, AgNP can enhance cross-linking, resulting in a higher swelling ratio for AgNP-chitosan-CMChi nanocomposite films compared to chitosan-CMChi composite films. This is due to the dispersion of Ag+ ions within the polymer network, which can induce network repulsion and ultimately lead to increased swelling in the system (Li et al., 2024).

Tensile strength is the maximum stress a film can withstand before breaking. This evaluation aims to determine the tensile strength and flexibility of the AgNP-chitosan-CMChi nanocomposite film. The tensile strength results are presented in Table 4. The tensile strength of the AgNP-chitosan-CMChi nanocomposite film ranges from 0.496 to 0.941 MPa as the effect of different AgNP concentrations on the tensile strength of the AgNP-chitosan-CMChi nanocomposite film. The results of the Tukey HSD post hoc test revealed that the concentration of AgNP 0.5 mM is significantly different from the concentrations of AgNP 0.25 mM and 0.375 mM. This improvement in the tensile strength of the film can be attributed to strong intermolecular interactions between the amino group ($-NH_2$) of chitosan and the generally negatively charged AgNPs, which result in a more robust structure (Mohamed and Madian, 2020).

The elongation at break value (%) is the percentage increase in length at which the film breaks (Savencu et al., 2021). The elongation at break evaluation aims to determine the film's toughness. The elongation at break value of the chitosan-CMChi composite film ranges from 55.12% to 61.47%. To assess the effect of differences in AgNP concentration on the elongation at break of the AgNP-chitosan-CMChi nanocomposite film, a one-way ANOVA statistical test was performed. The results showed no significant difference between formulas (p = 0.435; p >0.05). Based on the statistical test results, there is no interaction among AgNP concentrations. The elongation at break value increases with the addition of AgNPs. This can be attributed to the increasing number of AgNPs, which reduce the mobility of the chitosan matrix, making the film stiffer, more resistant to breaking, and less elastic (Rozilah et al., 2020).

Young's modulus describes the film's resistance to changes in length. The Young's modulus value is calculated by dividing the stress value by the strain value. The Young's modulus value of the AgNP-chitosan-CMChi nanocomposite film ranges from 2.163 to 7.492 N/mm^2. To assess the effect of differences in AgNP concentrations on the Young's modulus of the AgNP-chitosan-CMChi nanocomposite film, a one-way ANOVA statistical test was performed. To assess the impact of differences in AgNP concentrations. The statistical test results showed that the AgNP concentration at 0.25 mM differs significantly from that at 0.5 mM. The increase in the value of Young's modulus is attributed to the presence of cross-linking between AgNP and the polymer, which enhances tensile strength and makes the film more resistant to breaking (Dash et al., 2021).

The results for mechanical properties indicated a gradual increase as the concentration of AgNPs rose, suggesting their function as reinforcing nanofillers. When evenly distributed

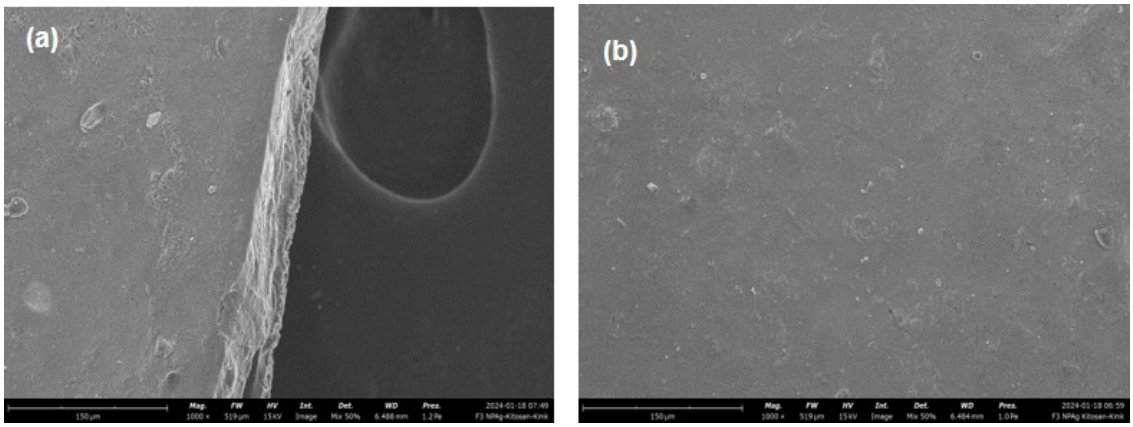

Figure 4. SEM Test Results of AgNP-Chitosan-CMChi Nanocomposite Film (a). Cross-Section and (b). Surface with 1000× Magnification

Table 4. Physical and Mechanical Properties for AgNP-Chitosan-CMChi Nanocomposite Film Formulations with Different AgNP Concentrations

Evaluation	Formula		
	Fn1	Fn2	Fn3
Thickness (mm)	0.18 ± 0.00	0.19 ± 0.02	0.22 ± 0.02
Foldability	>300	>300	>300
Moisture Content (%)	2.73 ± 0.57	6.31 ± 0.73	9.68 ± 0.35
Swelling Index (%)	561.45 ± 0.81	705.05 ± 0.74	912.13 ± 0.30
Tensile Strength (MPa)	0.496 ± 0.02	0.602 ± 0.07	0.941 ± 0.08
Elongation at break (%)	55.12 ± 6.83	60.97 ± 2.45	61.47 ± 6.06
Young's Modulus (N/mm^2)	2.163 ± 0.28	5.996 ± 2.60	7.492 ± 0.09

within the matrix, AgNPs promote more efficient stress transfer between the polymer network and the nanoparticles, thereby enhancing tensile strength and elastic modulus. However, at elevated concentrations, stronger interactions between the nanoparticles and polymer chains can limit chain mobility, leading to greater stiffness and reduced flexibility, which may cause the film to become more brittle. Furthermore, excessive AgNP content may promote particle aggregation, forming stress concentration sites that could compromise long-term structural stability. Thus, although incorporating AgNPs strengthens the film, optimizing their concentration is essential to achieve an appropriate balance between mechanical reinforcement and flexibility (Islam et al., 2025; Mebed et al., 2026; Sati et al., 2025).

3.4 Antibacterial Test of Nanocomposite Film

The antibacterial activity test was conducted in vitro using the diffusion method. This method determines a substance's antibacterial activity was evaluated by measuring the diameter of the inhibition zone observed. The test bacteria used were *Propionibacterium acnes* (ATCC 11827), a gram-positive, anaerobic bacterium that causes acne (Jawetz et al., 2008). The antibacterial activity of the AgNP-chitosan-CMChi films was evaluated by the agar diffusion method, which is widely used for qualitative screening of antimicrobial performance in solid materials such as films and coatings. The agar diffusion assay provides a relative indication of the inhibitory effect through the measurement of inhibition zones formed by the diffusion of active components from the film into the surrounding agar medium. This method is particularly appropriate for intact films because it reflects the release and diffusion behavior of the active agents within the polymer matrix, without requiring the material to be dissolved or dispersed in liquid, which can alter its structure and properties (Hossain, 2024; Savencu et al., 2021). In contrast, MIC and time-kill assays are designed for liquid culture systems in which the sample is fully solubilized or dispersed and may not be representative of the activity of solid films in their native form.

The antibacterial activity results for the nanocomposite film (Figure 5) and the visual observation in Figure 6 showed that the average inhibition zone diameter ranged from 7.98 to 14.17 mm. The inhibition diameter zone increased with increasing AgNP concentration. However, there was a slight decrease in the diameter of the inhibition zone for Fn3, although this was not statistically significant. This was due to an effect on the nanoparticles' shape, since different particle

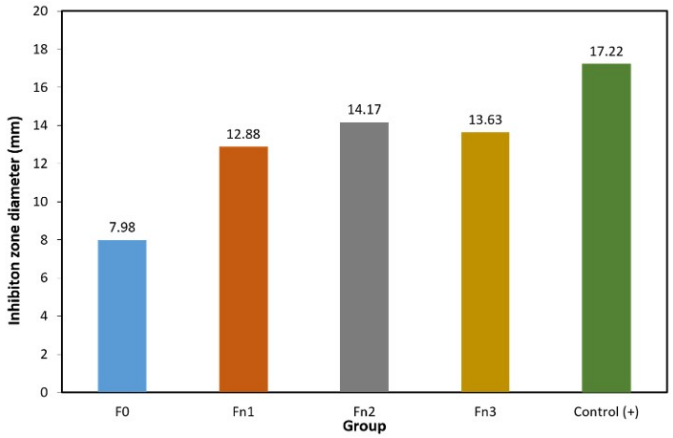

Figure 5. Antibacterial Activity of F0 (Chitosan 1.5%: CMChi 1.5%), Fn1 (Chitosan 1.5%: CMChi 1.5%: AgNP 0.25mM), Fn2 (Chitosan 1.5%: CMChi 1.5%; AgNP 0.375mM), Fn3 (Chitosan 1.5%: CMChi 1.5%: AgNP 0.5mM), and the Positive Control (Clindamycin) Against *Propionibacterium acnes*

shapes can yield different antibacterial activities (Abbaszadegan et al., 2015). According to the results of the Tukey HSD post hoc test, it is evident that the composite film without AgNP is significantly different from the nanocomposite film formulas with AgNP. Increasing NPAg in the nanocomposite film enhances antibacterial activity. Compared to films that do not contain AgNP (Fn0), the AgNP-chitosan-CMChi nanocomposite film exhibited a larger inhibition zone diameter than the chitosan-CMChi composite film.

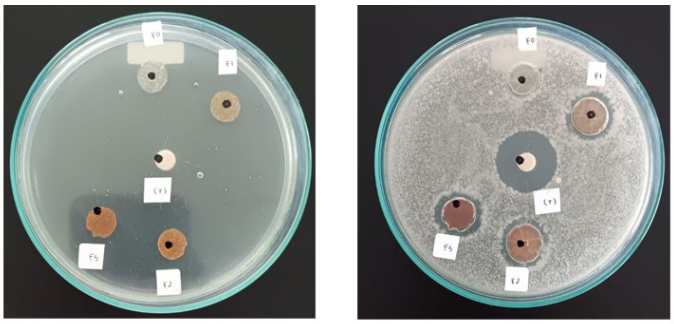

Figure 6. Antibacterial Activity Test Results of Fn0 (Chitosan 1.5%: CMChi 1.5%), Fn1 (Chitosan 1.5%: CMChi 1.5%: AgNP 0.25mM), Fn2 (Chitosan 1.5%: CMChi 1.5%; AgNP 0.375mM), Fn3 (Chitosan 1.5%: CMChi 1.5%: AgNP 0.5mM), and Positive Control (Clindamycin) Against *Propionibacterium acnes*

The antibacterial performance of the AgNP-chitosan-CMChi films increased with higher nanoparticle concentrations, as reflected by the larger inhibition zone diameters observed in the agar diffusion test. Films containing greater amounts of AgNPs produced wider clear zones, indicating stronger antimicrobial activity. This effect is likely due to the increased release of silver ions (Ag^+) and the presence of more nanoparticles, which can attach to bacterial cell walls, disturb membrane integrity, and promote the formation of reactive oxygen species (ROS), ultimately leading to bacterial cell death.

Nevertheless, at very high concentrations, AgNPs may aggregate, which can reduce their effective diffusion and direct interaction with bacterial cells. These findings emphasize the importance of optimizing nanoparticle loading to maximize antibacterial performance while ensuring proper dispersion within the polymer matrix. Comparable concentration-dependent antibacterial effects of AgNPs have also been documented in earlier studies (Darvish and Ajji, 2021).

4. CONCLUSIONS

The combination of AgNP with the chitosan–CMChi polymer in the AgNP-chitosan-CMChi nanocomposite film exhibited better characteristics compared to the film without AgNP, as indicated by improved mechanical properties such as higher tensile strength, elongation at break, and Young's modulus. Furthermore, the AgNP–chitosan–CMChi nanocomposite film demonstrated vigorous antibacterial activity against the gram-positive bacterium *Propionibacterium acnes (P. acnes)*.

5. ACKNOWLEDGMENT

Universitas Airlangga financially supported this research through Penelitian Unggulan Fakultas Grant with contract number 989/UN3.1.5/PT/2021.

REFERENCES

Abbasian, M., L. Rastogi, and S. K. Kora (2020). Morphological and Structural Evaluation of Polymer–AgNP Nanocomposites Using Advanced Imaging Techniques. *Materials Today Communications*, **25**; 101561

Abbaszadegan, A., Y. Ghahramani, A. Golami, B. Hemmateenejad, S. Dorostkar, M. Nabavizadeh, and H. Sharghi (2015). Sex and Proteinuria of Mice. *Proceedings of the Society for Experimental Biology and Medicine*, **48**(2); 395–400

Abraham, A., P. A. Soloman, and V. O. Rejini (2016). Preparation of Chitosan-Polyvinyl Alcohol Blends and Studies on Thermal and Mechanical Properties. *Procedia Technology*, **24**; 741–748

Alafandi, L., R. Nasaruddin, A. Aziz, N. Engliman, and M. Mastuli (2021). Green Synthesis of Silver Nanoparticles Using Coffee Extract for Catalysis. *Malaysian NANO-An International Journal*, **1**(2); 13–25

Alshamari, Y. M. G., H. Z. Alkhathlan, P. Karuppiah, M. Khan, E. Y. Danish, A. Aqel, S. F. Adil, and M. R. Shaik (2026). Structural Analysis and Antimicrobial Assessment of Bioinspired Silver Nanoparticles from Ferula Communis; 1–20

Angastiniotis, N. C., S. Christopoulos, K. C. Petallidou, A. M. Efstathiou, and A. Othonos (2021). Controlling the Optical Properties of Nanostructured Oxide-Based Polymer Films. *Scientific Reports*; 1–8

Awaluddin, N., S. Awaluddin, A. Awaluddin, and A. Suryani (2022). Formulation and Test of Antibacterial Activity of Antiacne Patch Preparations of Centella Asiatica Leaf Ethanol Extract Against the Growth of *Propionibacterium Acnes*. page 46

Bahsaine, K., E. Allaoui, H. Benzeid, E. Achaby, N. Zari, and R. Bouh (2023). Chitosan/Polyvinyl Alcohol-Based Films for Food Packaging Applications; 33294–33304

Cazón, P., G. Velazquez, J. A. Ramírez, and M. Vázquez (2017). Polysaccharide-Based Films and Coatings for Food Packaging: A Review. *Food Hydrocolloids*, **68**; 136–148

Ceballos, R. L., C. von Bilderling, L. Guz, C. Bernal, and L. Famá (2021). Effect of Greenly Synthetized Silver Nanoparticles on the Properties of Active Starch Films Obtained by Extrusion and Compression Molding. *Carbohydrate Polymers*, **261**; 117871

Chadha, R., N. Maiti, and S. Kapoor (2014). Reduction and Aggregation of Silver Ions in Aqueous Citrate Solutions. *Materials Science and Engineering C*, **38**(1); 192–196

Danaei, M., M. Dehghankhold, S. Ataei, F. H. Davarani, R. Javanmard, A. Dokhani, S. Khorasani, et al. (2018). Impact of Particle Size and Polydispersity Index on the Clinical Applications of Lipidic Nanocarrier Systems. *Pharmaceutics*; 1–17

Darvish, M. and A. Ajji (2021). Effect of Polyethylene Film Thickness on the Antimicrobial Activity of Embedded Zinc Oxide Nanoparticles. *ACS Omega*, **6**(40); 26201–26209

Dash, K. K., A. Kumar, S. Kumari, and M. A. Malik (2021). Silver Nanoparticle Incorporated Flaxseed Protein-Alginate Composite Films: Effect on Physicochemical, Mechanical, and Thermal Properties. *Journal of Polymers and the Environment*, **29**(11); 3649–3659

Dayarian, S., A. Zamani, A. Moheb, and M. Masoomi (2014). Physico-Mechanical Properties of Films of Chitosan, Carboxymethyl Chitosan, and Their Blends. *Journal of Polymers and the Environment*, **22**(3); 409–416

Elgharbawy, A. S., A. M. E. Demerdash, W. A. Sadik, M. A. Kasaby, A. H. Lotfy, and A. I. Osman (2024). Enhancing the Biodegradability, Water Solubility, and Thermal Properties of Polyvinyl Alcohol through Natural Polymer Blending: An Approach toward Sustainable Polymer Applications. **16**(15); 2141

Fithri, N. A., A. Fadilah, A. Pratiwi, S. S. Alisyahbana, M. F. Alhafiz, and N. Puan (2025). *Uncaria gambir* Based Green Synthesis of Inorganic Nanoparticles for Photothermal Induced Thrombolytic and Antibacterial Applications. **10**(1); 303–312

Gurvich, V. and M. Naumova (2021). SS Symmetry Logical Contradictions in the One-Way ANOVA and Tukey–Kramer Multiple Comparisons Tests with More Than Two Groups of Observations. **13**(8); 1387

Hadi, Z., A. H. Navarchian, and M. Rafienia (2023). Synthesis of pH-Responsive Carboxymethyl Chitosan for Encapsulating Tetracycline-HCl: Morphology, Drug Release Behavior and Antibacterial Activity of Microcapsules. *Journal of Drug Delivery Science and Technology*, **84**; 104462

Harun-ur Rashid, M. and T. Foyez (2025). Recent Advances of Silver Nanoparticle-Based Polymer Nanocomposites for Biomedical Applications. *RSC Advances*; 8480–8505

He, X., H. Xu, and H. Li (2015). Cr(VI) Removal from Aqueous Solution by Chitosan/Carboxymethyl Cellulose/Silica Hybrid Membrane; 234–240

Hoseini, B., M. R. Jaafari, A. Golabpour, A. Abbas, M. Borojeni, M. Karimi, and S. Eslami (2023). Application of Ensemble Machine Learning Approach to Assess the Factors Affecting Size and Polydispersity Index of Liposomal Nanoparticles. *Scientific Reports*; 1–11

Hossain, T. J. (2024). Methods for Screening and Evaluation of Antimicrobial Activity: A Review of Protocols, Advantages, and Limitations. **14**(2); 97–115

Islam, R., S. Maparathne, P. Chinwangso, and T. R. Lee (2025). Review of Shape-Memory Polymer Nanocomposites and Their Applications. **15**(5); 2419

Jawetz, Melnick, and Adelberg (2008). *Mikrobiologi Kedokteran*. 23 edition

Karki, S., H. Kim, S. J. Na, D. Shin, K. Jo, and J. Lee (2016). Thin Films as an Emerging Platform for Drug Delivery. *Asian Journal of Pharmaceutical Sciences*, **11**(5); 559–574

Kinoan, C. M. (2025). Sustainable Production and Antibacterial Efficacy of Silver Nanoparticles on Cellulose Nanofibers from Mushroom Waste. *RSC Advances*; 19726–19740

Kora, S. and L. Rastogi (2021). Recent Insights on Characterization of Biogenic Silver Nanoparticles in Polymer Matrices. *Colloid and Interface Science Communications*, **41**; 100369

Li, C., K. Wang, F. Li, and D. Xie (2024). Green Fabrication, Characterization and Antimicrobial Activities of AgO/Ag/-Carboxymethyl Chitosan-Graphene Oxide Films. *Arabian Journal of Chemistry*, **17**(1); 105380

Li, H. (2023). Use of TEM–EDS for Confirming Nanoparticle Distribution in Polymeric Nanocomposites. *Micron*

Madaniyah, L., S. Fiddaroini, E. K. Hayati, and A. Sabarudin (2025). Stability of Biologically Synthesized Silver Nanoparticles (AgNPs) Using *Acalypha Indica* L. Plant Extract as Bioreductor and Their Potential as Anticancer Agents Against T47D. **10**(1); 101–110

Mebed, A. M., A. H. Mohsen, D. J. Hassan, N. A. Ali, S. I. Hussein, F. T. M. Noori, A. M. Abd-Elnaiem, A. M. Alraih, and R. F. Abdelbaki (2026). A Flexible, Antibacterial Platform: Silver-Tuned Polyvinyl Alcohol with Enhanced Opto-Mechanical and Electrical Properties; 1–24

Mohamed, N. and N. G. Madian (2020). Evaluation of the Mechanical, Physical and Antimicrobial Properties of Chitosan Thin Films Doped with Greenly Synthesized Silver Nanoparticles. *Materials Today Communications*, **25**; 101372

Montgomery, D. C. (2019). *Design and Analysis of Experiments*. Wiley, 10 edition

Mulyana, S. D., R. Sari, and A. S. Rijal (2024). Green Synthesis of Silver Nanoparticles with Bioreductant from Lime Juice Powder (Citrus Aurantifolia): Effect of Concentration and pH. *Indonesian Journal of Chemistry*, **24**(5); 1445–1455

Nishigaki, M., K. Kawahara, M. Nawa, M. Futamura, M. Nishimura, K. Matsuura, K. Kitaichi, Y. Kawaguchi, T. Tsukioka, K. Yoshida, and Y. Itoh (2012). Development of Fast Dissolving Oral Film Containing Dexamethasone as an Antiemetic Medication: Clinical Usefulness. *International Journal of Pharmaceutics*, **424**(1-2); 12–17

Nugraheni, A. D., D. Purnawati, and A. Kusumaatmaja (2018). Physical Evaluation of PVA/Chitosan Film Blends with Glycerine and Calcium Chloride. *Journal of Physics: Conference Series*, **1011**(1); 012052

Ounkaew, A., P. Kasemsiri, K. Jetsrisuparb, H. Uyama, Y. I. Hsu, T. Boonmars, A. Artchayasawat, J. T. N. Knijnenburg, and P. Chindaprasirt (2020). Synthesis of Nanocomposite Hydrogel Based Carboxymethyl Starch/Polyvinyl Alcohol/-Nanosilver for Biomedical Materials. *Carbohydrate Polymers*, **248**; 116767

Psimadas, D., P. Georgoulias, V. Valotassiou, and G. Loudos (2012). Molecular Nanomedicine Towards Cancer. *Journal of Pharmaceutical Sciences*, **101**(7); 2271–2280

Ramezani, E., M. Jahanshahi, H. Hamishehkar, and M. Mohammadi (2022). Visualization Challenges of Metallic Nanoparticles Embedded in Biopolymer Films. *Journal of Applied Polymer Science*, **139**(25); 52229

Rozilah, A., C. N. Aiza Jaafar, S. M. Sapuan, I. Zainol, and R. A. Ilyas (2020). The Effects of Silver Nanoparticles Compositions on the Mechanical, Physicochemical, Antibacterial, and Morphology Properties of Sugar Palm Starch Biocomposites for Antibacterial Coating. *Polymers*, **12**(11); 2605

Sati, A., T. N. Ranade, H. Khader, A. Yasin, and A. Pratap (2025). Silver Nanoparticles (AgNPs): Comprehensive Insights into Bio/Synthesis, Key Influencing Factors, Multifaceted Applications, and Toxicity-A 2024 Update. *ACS Omega*, **10**(8); 7549–7582

Savencu, I., S. Iurian, A. Porfire, C. Bogdan, and I. Tomuță (2021). Review of Advances in Polymeric Wound Dressing Films. *Reactive and Functional Polymers*, **168**; 105059

Susilowati, E., S. R. D. Ariani, L. Mahardiani, and L. Izzati (2021). Synthesis and Characterization of Chitosan Film with Silver Nanoparticle Addition as a Multiresistant Antibacterial Material. *JKPK (Jurnal Kimia dan Pendidikan Kimia)*, **6**(3); 371

Takeuchi, Y., K. Umemura, K. Tahara, and H. Takeuchi (2018). Formulation Design of Hydroxypropyl Cellulose Films for Use as Orally Disintegrating Dosage Forms. *Journal of Drug Delivery Science and Technology*, **46**; 93–100

Tang, C., B. Zhao, J. Zhu, X. Lu, and G. Jiang (2022). Preparation and Characterization of Chitosan/Sodium Cellulose Sulfate/Silver Nanoparticles Composite Films for Wound Dressing. *Materials Today Communications*, **33**; 104192

Wardhono, E. Y., M. P. Pinem, S. Susilo, B. J. Siom, A. Sudrajad, A. Pramono, Y. Meliana, and E. Gu (2022). Modification of Physio-Mechanical Properties of Chitosan-Based Films via Physical Treatment Approach. **14**(23); 5216

Yang, J., Y. Chen, L. Zhao, Z. Feng, K. Peng, A. Wei, Y. Wang, Z. Tong, and B. Cheng (2020). Preparation of a Chitosan/-Carboxymethyl Chitosan/AgNPs Polyelectrolyte Composite Physical Hydrogel with Self-Healing Ability, Antibacterial Properties, and Good Biosafety Simultaneously, and Its Application as a Wound Dressing. *Composites Part B: Engineering*, **197**; 108139

Zar, J. H. (2010). *Biostatistical Analysis*. Pearson Education, 5 edition

Zhang, D., W. Zhou, B. Wei, X. Wang, R. Tang, J. Nie, and J. Wang (2015). Carboxyl-Modified Poly(Vinyl Alcohol)-Crosslinked Chitosan Hydrogel Films for Potential Wound Dressing. *Carbohydrate Polymers*, **125**; 189–199

Zimet, P., A. W. Mombru, D. Mombru, A. Castro, J. P. Villanueva, H. Pardo, and C. Rufo (2019). Physico-Chemical and Antilisterial Properties of Nisin-Incorporated Chitosan/-Carboxymethyl Chitosan Films. *Carbohydrate Polymers*, **219**; 334–343

